VIP Colloids

DOI: 10.1002/ange.200705049

Controlling Colloidal Superparticle Growth Through Solvophobic Interactions**

*Jiaqi Zhuang, Huimeng Wu, Yongan Yang, and Y. Charles Cao**

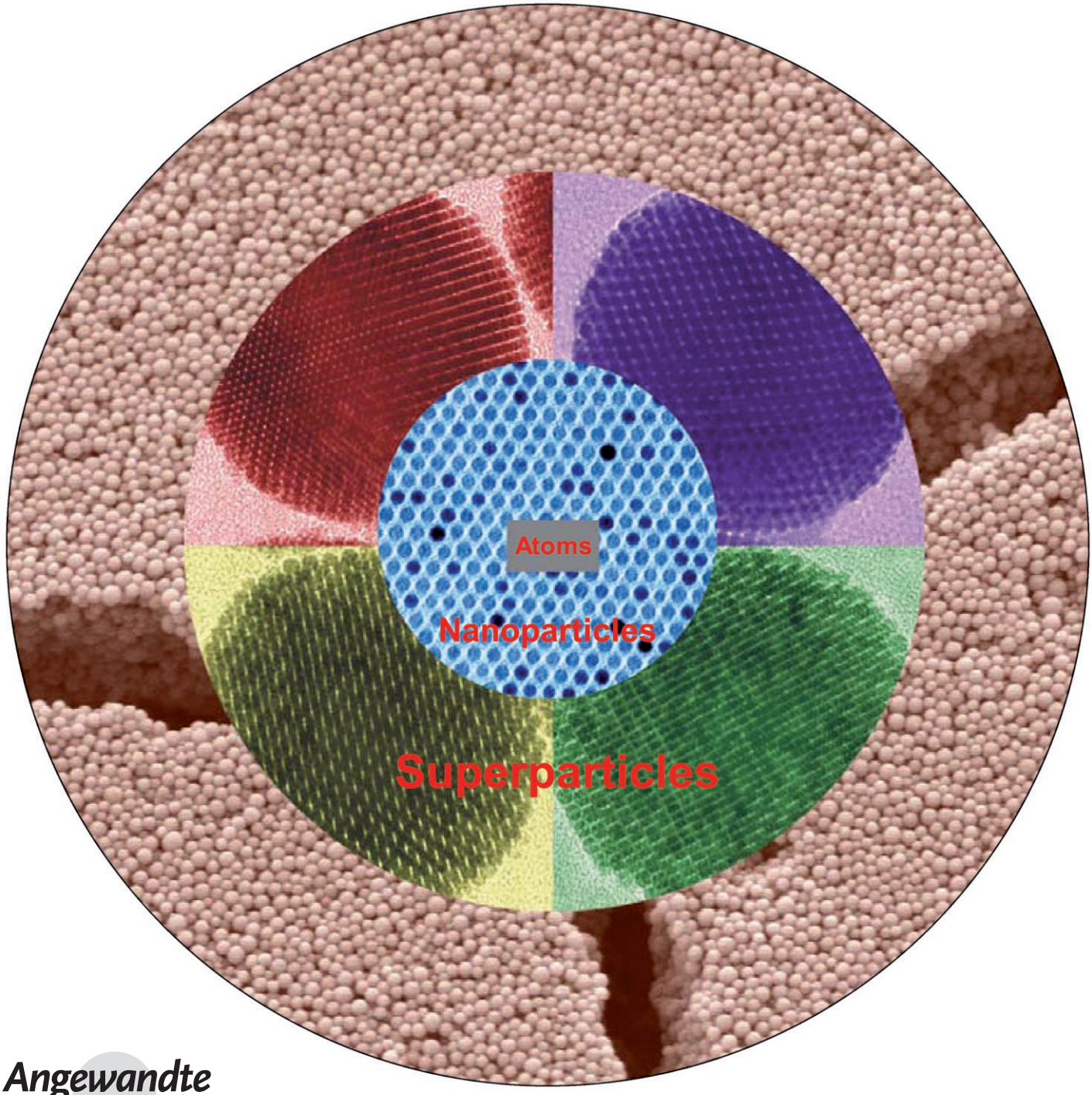

Assembly of nanoparticles (1–100 nm in diameter) into higher-order nanostructures such as superlattices may create an opportunity to manufacture materials with new physical, chemical, and mechanical properties,[1,2] which are important to applications ranging from biological labeling to solar cells.[3-5] This opportunity has motivated research efforts aimed at developing methods for making 2D and 3D nanoparticle assemblies with a variety of superlattice structures.[6] However, less is known about how to fabricate nanoparticle superlattices in the form of superparticles with well-controlled size and shape, which can be developed as a new type of building block in nanoscience. Herein, superparticles (SPs) refer to the colloidal particles made of nanoparticles through assembly.

Recently, Li and co-workers reported an approach for using the oil droplets in microemulsions as templates to grow nanoparticle assemblies.[7] The approach has led to the synthesis of high-quality SPs with well-controlled size and shape, and nanoparticles in the SPs exhibit long-range ordering at some orientations. More recently, we have developed a template-free, supramolecular chemistry approach for using solvophobic interactions to synthesize supercrystalline Fe_3O_4 SPs.[8] The SPs made by our approach possess a nearly perfect face-centered cubic (fcc) superlattice structure. These supercrystalline SPs exhibit superlattice fringes in low-resolution transmission electron microscopy (TEM) images, providing an interesting analogue to the lattice fringes of colloidal nanocrystals in high-resolution TEM images.[8] Herein we report that the formation of supercrystalline SPs in our synthesis follows Ostwald's rule,[9] which is a two-step process. On the basis of this new mechanistic understanding, we demonstrate that our approach can be extended to synthesize relatively monodispersed SPs with diameters from 120 to 560 nm. Furthermore, we show that the properties of these novel SPs can be tailored by doping with organic dyes.

Our synthesis of supercrystalline SPs involves preparing water-soluble nanoparticle micelles and then growing colloidal SPs from the nanoparticle micelles in ethylene glycol. In a typical experiment, nanoparticle micelles made from oleic acid functionalized Fe_3O_4 nanoparticles (5.8 nm in diameter) and dodecyltrimethylammonium bromide (DTAB) were injected into an ethylene glycol solution of poly(vinyl pyrrolidone) (PVP). The mixture was then heated to 80 °C and annealed for 6 h. The resulting SPs are 190 nm in diameter with a relative standard deviation of 17%. In polar solvents (e.g. ethanol and water), the SPs are highly dispersible and can form stable colloids.

Under low-resolution TEM, the SPs exhibit cross-fringe images that are identified as the on-axis superlattice-fringe patterns of a face-centered cubic (fcc) superlattice structure (Figure 1).[10] These patterns include the cross-fringe images

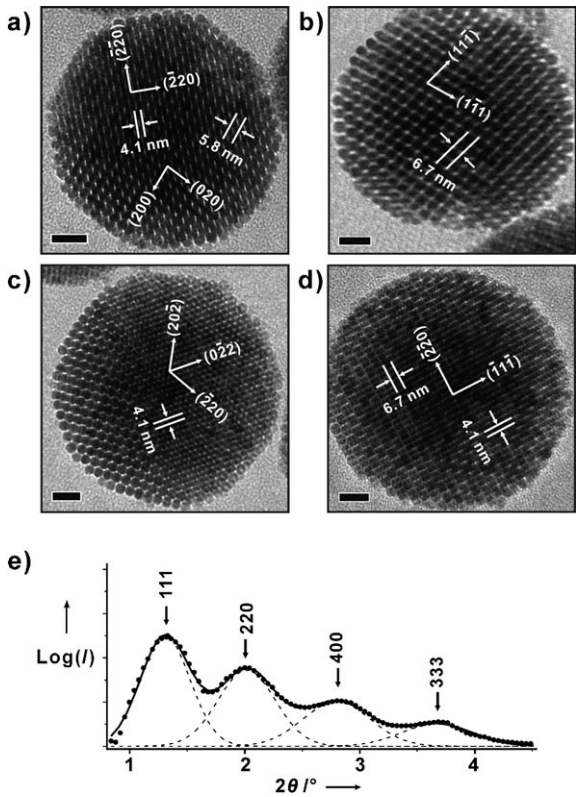

Figure 1. TEM images of SPs made of Fe_3O_4 nanoparticles (5.8 ± 0.2 nm in diameter) viewed along the zone axis of a) [001], b) [011] c) [111], and d) $[1\bar{1}\bar{2}]$. e) Small-angle XRD pattern of a sample with SPs of 190 nm in diameter.[12] Experimental data are shown as dots; fitting curve is shown as a solid line. Scale bars: 20 nm.

viewed along the [001], [011], [111], and even $[1\bar{1}\bar{2}]$ zone axes (Figure 1 a–d).[10] Like atomic lattice cross fringes from a high-resolution TEM measurement, these superlattice-fringe images are also acquired under an objective-lens defocus.[10] The origin of these superlattice fringes is likely from electron phase contrast owing to the interference among the incident beam and small-angle diffraction beams through the supercrystalline SPs.[8] The identification of superlattice fringes is important for understanding the 3D packing structure of nanoparticle building blocks in their assemblies.

Taken together, the spacing and geometry of the cross fringes in these TEM images indicate that the fcc nanoparticle superlattice has a lattice constant of 11.7 ± 0.2 nm.[11] The superlattice structure was further investigated by an ensemble measurement of these SPs using small-angle X-ray diffraction (XRD). The XRD pattern exhibits four distinguishable peaks that are located at the positions corresponding to the Bragg reflections from planes specified by the Miller indices as (111), (220), (400), and (333) of the fcc superlattice (Fig-

[*] Dr. J. Zhuang, H. Wu, Dr. Y. Yang, Prof. Y. C. Cao
Department of Chemistry
University of Florida
Gainesville, FL 32611 (USA)
Fax: (+1) 352-392-0588
E-mail: cao@chem.ufl.edu

[**] We thank Kerry Siebein for TEM measurements. Y.C.C. acknowledges the NSF (DMR-0645520 Career Award), ONR (N00014-06-1-0911) and the American Chemical Society Petroleum Research Fund (42542-G10) for support of this research.

Supporting information for this article is available on the WWW under http://www.angewandte.org or from the author.

ure 1e). The lattice constant determined from this XRD pattern is 11.9 ± 0.3 nm,[12] which is in excellent agreement with the value of 11.7 ± 0.2 nm from the TEM measurements.

On the basis of detailed mechanistic studies, we have identified two major steps in the synthesis of these supercrystalline colloidal SPs: i) aggregation and ii) crystallization (Figure 2a). TEM shows that the Fe_3O_4 particle micelles were

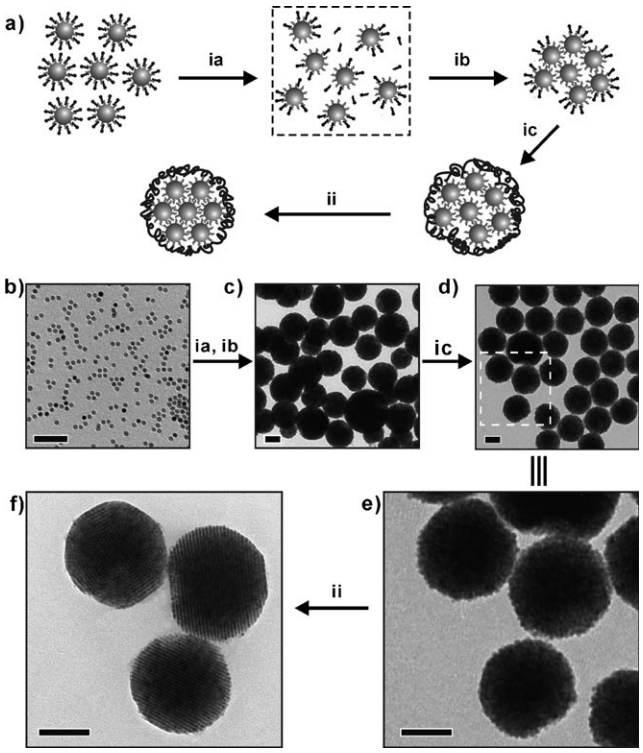

Figure 2. a) A schematic representation of the proposed formation mechanism of supercrystalline SPs. b) A TEM image of DTAB Fe_3O_4 nanoparticle micelles. c) A TEM image of SPs made without PVP at room temperature. d) A TEM image of SPs made with PVP at room temperature. e) An enlarged image of the inset in (d). f) A TEM image of SPs after annealing at 80 °C for 6 h. Scale bars: 50 nm (b), 100 nm (c–f). The synthesis stages are i) aggregation, and ii) crystallization. Enlarged images of (e) and (f) can be found in the Supporting Information (Figure S6).

monodispersed with a nearly identical size to their nonpolar-solvent-dispersible precursors (Figure S1 in the Supporting Information). These nanoparticle micelles are dispersible in aqueous solution owing to the hydrophobic van der Waals interactions between the hydrocarbon chain of the Fe_3O_4 nanoparticle ligands (oleic acid) and the hydrocarbon chain of the surfactant (DTAB).[13,14] The van der Waals interactions between nanoparticle ligands and surfactants were weakened after the nanoparticle-micelle solution was introduced into an ethylene glycol solution,[15] at which point nanoparticle micelles decomposed owing to the loss of DTAB molecules into the solution (Figure 2a).

As a result, solvophobic interactions between oleic acid functionalized nanoparticles and ethylene glycol solution were induced,[14,15] thus leading to the aggregation of nanoparticles and the formation of SPs (Figure 2). The mechanism was confirmed by ^{1}H NMR spectroscopic analyses (Figure 3). NMR spectra show that the Fe_3O_4 nanoparticle micelles were functionalized with both oleic acid and DTAB molecules at a ratio of 2.4:1 (Figure 3a). In contrast, the major ligands in the Fe_3O_4 SPs were only oleic acid; the amount of DTAB was not measurable in the Fe_3O_4 SPs (Figure 3b). These NMR spectroscopy results demonstrate that the loss of DTAB indeed occurs during the formation of SPs.

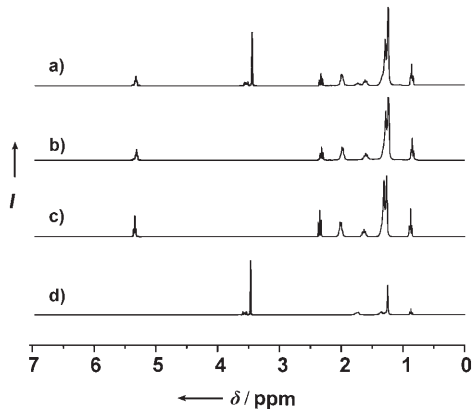

Figure 3. ^{1}H NMR spectra of a) the organic ligands on the Fe_3O_4 micelles, b) the organic ligands on the Fe_3O_4 SPs, c) oleic acid, and d) DTAB.[12]

Surprisingly, the SP formation is a very rapid process. TEM studies show that nearly all of the 5.8-nm Fe_3O_4 nanoparticles grew into SPs within 1 min after the injection of nanoparticle micelles, and then afterwards the size of the SPs did not change substantially (see Figure S2 in the Supporting Information). Furthermore, the repulsive solvophobic interaction is likely the reason that the SPs adopted a spherical shape, in which the particles can have the minimum surface energy.[14] Moreover, the addition of PVP has no substantial effect on the size of the SPs (Figure 2c,d), which further confirms that solvophobic interactions are the major driving force behind the formation of SPs.

To further demonstrate that the solvophobic interaction is important for nanoparticle aggregation, cetyltrimethylammonium bromide (CTAB) was used to replace DTAB as a surfactant for making Fe_3O_4 nanoparticle micelles. In ethylene glycol, these CTAB nanoparticle micelles are much more stable than those made of DTAB, because CTAB has a lower solubility in ethylene glycol and a stronger van der Waals interaction with the nanoparticle ligands (i.e. oleic acid) than DTAB.[14] Therefore, no sufficient solvophobic interaction can be induced between the oleic acid functionalized nanoparticles and ethylene glycol solvent.[12] Indeed, TEM shows that CTAB nanoparticle micelles remained nearly unchanged in ethylene glycol even at 80 °C for 6 h, and no spherical nanoparticle assembly was formed (see Figure S3 in the Supporting Information).

Further mechanistic studies show that the primary role of PVP is as a capping reagent to stabilize these SPs through repulsive steric interactions.[14] Other capping reagents such as gelatin can also play a similar role. Without these capping

reagents, SPs were unstable, and their structures easily collapsed during annealing at 80 °C (see Figure S4 in the Supporting Information). Moreover, TEM shows that the annealing treatment is important to the formation of single-supercrystalline SPs. Before annealing, the spherical colloidal SPs don't exhibit superlattice fringes (Figure 2e), thus indicating that the nanoparticles are not perfectly ordered in these SPs (or the spherical SPs are in an "amorphous" phase). This observation is consistent with the fact that SP formation is a very rapid process in which nanoparticle building blocks have not yet located their equilibrium positions. After annealing, the spherical SPs show very clear superlattice fringes (Figure 2f). These results suggest that the annealing treatment is accompanied by a crystallization process to rearrange Fe_3O_4 nanoparticles into a single-supercrystal phase inside these SPs.[16] In the crystallization step, Fe_3O_4 nanoparticles with a narrow size distribution and sufficient surface passivation were found to be important to the formation of the single-supercrystal structure.

These mechanistic studies reveal that in their formation, supercrystalline SPs go through an amorphous phase before the final supercrystalline phase is reached. Such a formation process follows Ostwald's rule, because the amorphous phase is normally the one which is nearest in free energy to the mother solution phase.[9] Moreover, mechanistic studies suggest that the solvophobic interactions between the nanoparticles and ethylene glycol solution is the major driving force for the formation of the spherical amorphous SPs, which have a nearly identical size and shape to the final supercrystalline SPs. Further studies show that fine-tuning the solvophobic interaction allows control of the size of these SPs.

In our previous studies of organic-phase synthesis of CdS nanocrystals from molecular precursors, we found that the number of nuclei can be controlled by the reactivity of molecular precursors: higher precursor reactivity led to fewer nuclei and thus to a larger final particle size, and vice versa.[17] We found that this principle is transferable to size control of spherical SPs. In this supramolecular chemistry synthesis case, the higher "reactivity" of nanoparticle precursors corresponds to stronger solvophobic interaction between the nanoparticles and ethylene glycol solution, which can be achieved by using a smaller molar ratio between DTAB and Fe_3O_4 nanoparticles. Applying this principle did lead to the formation of larger SPs (Figure 4). On the other hand, smaller SPs were also made according to the same principle using lower-reactivity nanoparticle precursors (Figure 4).

The development of the supramolecular chemistry synthesis of supercrystalline SPs is important for three fundamental reasons. First, the synthesis approach can be generalized for making supercrystalline colloidal SPs from nonpolar-solvent-dispersible nanoparticles with other sizes and chemical compositions, such as metals, metal oxides, and semiconductors (Figure 5a–c). Second, the properties of these supercrystalline colloidal SPs can be easily modified by doping with organic molecules, such as dye sensitizers. For example, rhodamine-6G-doped supercrystalline colloidal SPs (made of 5.4-nm gold nanoparticles) exhibit strong surface-enhanced Raman scattering (Figure 5d), owing to electromagnetic field enhancement from gold SPs.[18] Third, because of their excellent stability in polar solvents, these colloidal SPs can be further assembled, through solution processing, into more complex and hierarchically ordered materials in which new properties may occur.

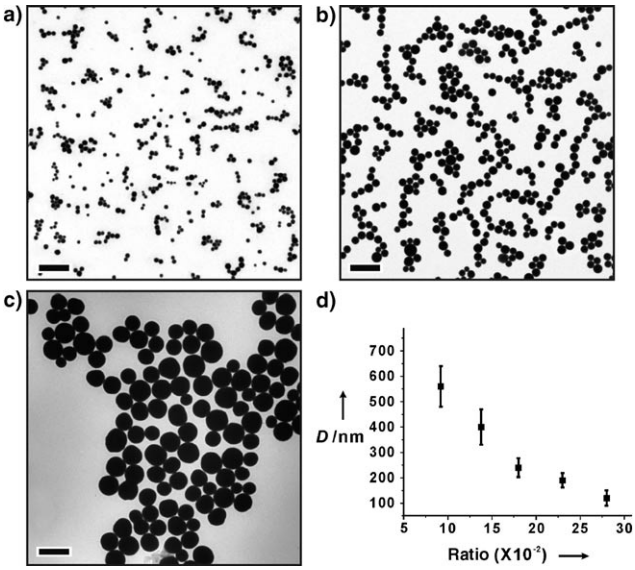

Figure 4. TEM images of a) SPs with a diameter of 120 nm and a standard deviation of 19%, b) SPs with a diameter of 190 nm and a standard deviation of 17%, c) SPs with a diameter of 560 nm and a standard deviation of 15%. d) A plot of SP size as a function of the molar ratio between DTAB surfactant and the 5.8 nm Fe_3O_4 nanoparticles. Scale bars: 1 μm.

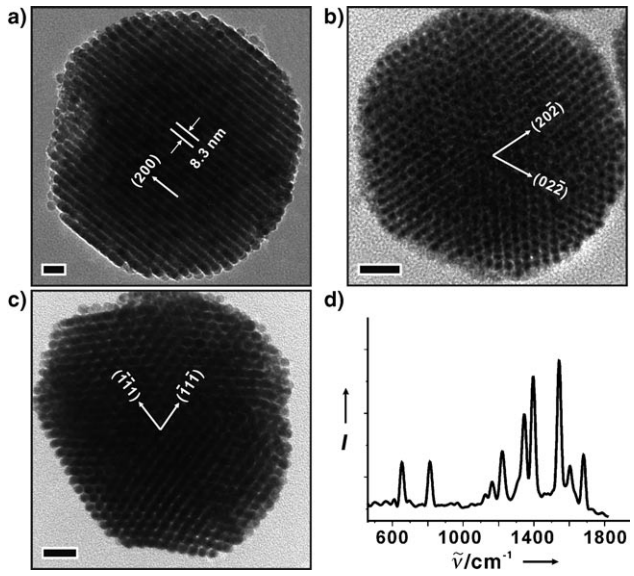

Figure 5. TEM images of a) a SP made of Fe_3O_4 nanoparticles with a diameter of 8.9 ± 0.4 nm, showing the $\{200\}_{SL}$ superlattice-fringes with a spacing of 8.3 nm; b) a SP made of CdSe nanoparticles with a diameter of 6.3 ± 0.3 nm; the image is viewed along the [111] axis of the superlattice, showing $\{022\}_{SL}$ superlattice-fringes with a spacing of 4.3 nm; c) a SP made of gold nanoparticles with a diameter of 5.4 ± 0.3 nm, viewed along the [011] zone axis, showing $\{111\}_{SL}$ fringes with a spacing of 6.2 nm. d) The Raman spectrum of rhodamine-6G-doped supercrystalline colloidal SPs made of gold nanoparticles with a diameter of 5.4 ± 0.3 nm. Scale bars: 20 nm.

Experimental Section

Fe_3O_4 SPs were synthesized according to the following procedure. In a typical experiment, a chloroform solution of oleic acid functionalized Fe_3O_4 nanoparticles (5.8 ± 0.2 nm in diameter, 28 μM, 1.0 mL) was mixed with an aqueous dodecyltrimethylammonium bromide solution (DTAB, 65 mM, 1.0 mL), and a clear nanoparticle-micelle aqueous solution was obtained by evaporating the chloroform. Under vigorous stirring, the nanoparticle-micelle solution was injected into an ethylene glycol solution of poly(vinyl pyrrolidone) (PVP) (2.0 mM, 5.0 mL). The resulting mixture was heated to 80 °C at 10 °C min^{-1} and was annealed for 6 h. Then the reaction solution was cooled to room temperature. Colloidal SPs were isolated from the reaction solution by centrifugation, with a typical yield of about 70 %. The size-controlled synthesis of superparticles was performed by a procedure similar to that described above, but using different molar ratios of DTAB and nanoparticles. The synthesis of colloidal SPs from 8.9-nm Fe_3O_4, 6.3-nm CdSe, and 5.4-nm gold nanoparticles was carried out using a procedure similar to that described above, except that gelatin was used as an additional passivation ligand in the synthesis of gold SPs.[12]

^{1}H NMR spectroscopy (Varian Mercury NMR Spectrometer, 300 MHz) was used to identify the ligands on the Fe_3O_4 nanoparticle micelles and the SPs.[12] Fe_3O_4 nanoparticle micelles were isolated from an aqueous solution by centrifugation (12500 *g*). The resulting black precipitate (100 mg) was fully digested using HCl (12.5 M, 5 mL); water and excess HCl were then removed by rotary evaporation. The resulting yellow, oily residue was extracted using $CHCl_3$ (5 mL) and the undissolved part was removed using a syringe filter (0.2 μm). Afterwards, $CHCl_3$ was evaporated, and the resulting mixture was redissolved in $CDCl_3$ (0.8 mL) for ^{1}H NMR spectroscopy measurement. The sample preparation for the analysis of the Fe_3O_4 SPs was carried out using a similar procedure.

Received: October 31, 2007
Published online: January 31, 2008

Keywords: colloids · nanoparticles · self-assembly · superlattices

[1] a) G. Markovich, C. P. Collier, S. E. Henrichs, F. Remacle, R. D. Levine, J. R. Heath, *Acc. Chem. Res.* **1999**, *32*, 415 – 423; b) E. V. Shevchenko, D. V. Talapin, A. L. Rogach, A. Kornowski, M. Haase, H. Weller, *J. Am. Chem. Soc.* **2002**, *124*, 13958 – 13958.

[2] a) E. W. Edwards, D. Y. Wang, H. Möhwald, *Macromol. Chem. Phys.* **2007**, *208*, 439—445; b) M. Brust, *Nat. Mater.* **2005**, *4*, 364 – 365.

[3] a) N. L. Rosi, C. A. Mirkin, *Chem. Rev.* **2005**, *105*, 1547 – 1562; b) C. Sonnichsen, B. M. Reinhard, J. Liphardt, A. P. Alivisatos, *Nat. Biotechnol.* **2005**, *23*, 741 – 745.

[4] a) R. C. Jin, J. E. Jureller, H. Y. Kim, N. F. Scherer, *J. Am. Chem. Soc.* **2005**, *127*, 12482 – 12483; b) A. Courty, A. Mermet, P. A. Albouy, E. Duval, M. P. Pileni, *Nat. Mater.* **2005**, *4*, 395 – 398; c) X. Liu, L. Fu, S. Hong, V. P. Dravid, C. A. Mirkin, *Adv. Mater.* **2002**, *14*, 231 – 234; d) J. Zhao, J. A. Bardecker, A. M. Munro, M. S. Liu, Y. Niu, I. K. Ding, J. Luo, B. Chen, A. K. Y. Jen, D. S. Ginger, *Nano Lett.* **2006**, *6*, 463 – 476; e) G. A. Somorjai, R. M. Rioux, J. Grunes in *Clusters and Nano-Assemblies* (Eds.: P. Jena, S. N. Khanna, B. K. Rao), World Scientific, Singapore, **2005**, pp. 97 – 125.

[5] I. Gur, N. A. Fromer, M. L. Geier, A. P. Alivisatos, *Science* **2005**, *310*, 462 – 465.

[6] a) S. Sun, C. B. Murray, D. Weller, L. Folks, A. Moser, *Science* **2000**, *287*, 1989 – 1992; b) C. J. Kiely, J. Fink, M. Brust, D. Bethell, D. J. Schiffrin, *Nature* **1998**, *396*, 444 – 446; c) C. B. Murray, C. R. Kagan, M. G. Bawendi, *Science* **1995**, *270*, 1335 – 1338; d) E. V. Shevchenko, D. V. Talapin, N. A. Kotov, S. O'Brien, C. B. Murray, *Nature* **2006**, *439*, 55 – 59; e) M. Kalsin, M. Fialkowski, M. Paszewski, S. K. Smoukov, K. J. M. Bishop, B. A. Grazybowski, *Science* **2006**, *312*, 420 – 424; f) J. Sharma, R. Chhabra, Y. Liu, Y. Ke. H. Yan, *Angew. Chem.* **2006**, *118*, 744 – 749; *Angew. Chem. Int. Ed.* **2006**, *45*, 730 – 735.

[7] F. Bai, D. S. Wang, Z. Y. Huo, W. Chen, L. P. Liu, X. Liang, C. Chen, X. Wang, Q. Peng, Y. D. Li, *Angew. Chem.* **2007**, *119*, 6770 – 6773; *Angew. Chem. Int. Ed.* **2007**, *46*, 6650 – 6653.

[8] J. Q. Zhuang, H. M. Wu, Y. A. Yang, Y. C. Cao, *J. Am. Chem. Soc.* **2007**, *129*, 14166 – 14167.

[9] W. Ostwald, *Z. Phys. Chem. Stoechiom. Verwandtschaftsl.* **1897**, *22*, 289 – 330.

[10] D. B. Williams, C. B. Carter in *Transmission Electron Microscopy*, Plenum, New York, **1996**.

[11] D. McKie, C. McKie, *Crystalline Solids*, Wiley, New York, **1974**.

[12] See the Supporting Information.

[13] H. Y. Fan, E. Leve, J. Gabaldon, A. Wright, R. E. Haddad, C. J. Brinker, *Adv. Mater.* **2005**, *17*, 2587 – 2590.

[14] H. J. Butt, K. Graf, M. Kappl, *Physics and Chemistry of Interfaces*, Wiley-VCH, Weinheim, **2006**.

[15] a) M. Q. Zhu, L. Q. Wang, G. J. Exarhos, A. D. Q. Li, *J. Am. Chem. Soc.* **2004**, *126*, 2656 – 2657; b) E. Rabani, S. A. Egorov, *Nano Lett.* **2002**, *2*, 69 – 72.

[16] C. B. Murray, C. R. Kagan, M. G. Bawendi, *Annu. Rev. Mater. Sci.* **2000**, *30*, 545 – 610.

[17] Y. C. Cao, J. Wang, *J. Am. Chem. Soc.* **2004**, *126*, 14336 – 14337.

[18] G. C. Schatz, R. P. Van Duyne in *Handbook of Vibrational Spectroscopy* (Eds.: J. M. Chalmers, P. R. Griffiths), Wiley-VCH, New York, **2002**, pp. 759 – 774.

